Journal of Materials Chemistry A

PAPER

View Article Online
View Journal | View Issue

Cite this: J. Mater. Chem. A, 2015, 3, 13468

Hierarchically nanoporous $La_{1.7}Ca_{0.3}CuO_{4-\delta}$ and $La_{1.7}Ca_{0.3}Ni_xCu_{1-x}O_{4-\delta}$ ($0.25 \leq x \leq 0.75$) as potential cathode materials for IT-SOFCs†

Xiubing Huang, Tae Ho Shin, Jun Zhou and John T. S. Irvine*

Received 6th February 2015
Accepted 27th May 2015

DOI: 10.1039/c5ta00983a

www.rsc.org/MaterialsA

Hierarchically nanoporous materials based on layered perovskite oxides $La_{1.7}Ca_{0.3}Ni_xCu_{1-x}O_{4-\delta}$ ($x = 0$, 0.25, 0.50 or 0.75) have been synthesized by a facile citrate-modified evaporation-induced self-assembly (EISA) method. These $La_{1.7}Ca_{0.3}Ni_xCu_{1-x}O_{4-\delta}$ oxides have been evaluated as potential cathodes for intermediate-temperature solid oxide fuel cells (IT-SOFCs) with Ni–YSZ cermet supported type cells. It was found that $La_{1.7}Ca_{0.3}CuO_{4-\delta}$ cathode exhibits the maximum power density at high temperature (*e.g.*, 1.5 W cm^{-2} at 850 °C), while $La_{1.7}Ca_{0.3}Ni_{0.75}Cu_{0.25}O_{4-\delta}$ cathode shows the highest power density at intermediate temperature (*e.g.* 0.71 W cm^{-2} at 750 °C) using humidified H_2 and air as the fuel and oxidant, respectively. The electrochemical performance of single cells with $La_{1.7}Ca_{0.3}Ni_{0.75}Cu_{0.25}O_{4-\delta}$ cathode materials with different morphologies demonstrated better performance in the intermediate temperature range when using the cathode prepared by the citrate-modified EISA method, which has a bigger grain size, but with higher surface area and pore volumes.

Introduction

Solid oxide fuel cells (SOFCs) have been considered as one of the most advanced power generation technologies for environmentally friendly power generators due to their high energy conversion efficiency, fuel adaptability and so on.[1,2] However, their high operating temperatures (800–1000 °C) have brought in strict requirements (*e.g.*, avoiding chemical reactions and thermal expansion mismatch between electrodes and electrolyte) on the electrode and interconnect materials, which limit the commercialization and wide usage of SOFCs.[1,3] Consequently, extensive efforts have been devoted to the development of IT-SOFCs between intermediate-temperature range (500–750 °C) to improve long-term stability, provide more cell material choice and decrease costs.[4–8] However, the decrease of operating temperature usually leads to the reduction of electrical performance because of the polarization loss of the cathode.[9–12] Commercial cathode materials including Sr or Mn, like LSCF ($La_{1-x}Sr_xCo_yFe_{1-y}O_3$) and LSM ($La_{1-x}Sr_xMnO_3$), present cation segregation at the surface over the long term that would reduce the cathode reactivity and stability in oxygen reduction reactions (ORR).[13–18] Therefore, it is essential to develop effective cathode materials for IT-SOFCs with high electrochemical activity.

Some perovskite-type oxides have mixed ionic-electronic conducting (MIEC) and have been widely investigated as the cathode materials for IT-SOFCs due to their good performance for ORR.[19,20] Recently, MIECs based on layered perovskites with K_2NiF_4-type structure have received extensive interest as cathode materials for IT-SOFCs, owing to their relatively high oxygen ion diffusivity, rapid surface exchange property, and compatible thermal expansion coefficients with solid electrolytes.[20,21] Most of the studies have been focused on the oxygen over-stoichiometry layered perovskites, especially La_2NiO_4 based materials, which have been reported to have good ionic conductivity because of the interstitial oxygen.[22–25] However, the low electronic conductivity of La_2NiO_4 limits its further practical use as SOFC cathodes.[26]

In addition, as another archetypal material with K_2NiF_4 structure, layered La_2CuO_4 has previously been investigated for its electrical conduction properties, such as superconductivity at low temperature, and metallic/semi-conducting properties at room temperature.[27,28] According to many previous reports, introducing alkaline-earths (*e.g.*, Sr, Ca, Ba) at the La-site provides effective routes to further improve their electrical conductivity through formation of electron–holes, oxygen vacancies or interstitial oxygen.[28–31] Partially substituting Cu with other transition metals (*e.g.*, Ni) could also improve their ionic conductivity which would enhance the performance of these substituted La_2CuO_4 oxides as cathode materials of SOFC,[32,33] however, the Sr-doped La_2CuO_4 exhibits the issues of

School of Chemistry, University of St Andrews, St Andrews, Fife, UK. E-mail: jtsi@st-andrews.ac.uk; Fax: +44 (0)1334463808; Tel: +44 (0)133463680

† Electronic supplementary information (ESI) available: Rietveld refinements from XRD patterns, SEM and TEM images, N_2 adsorption/desorption isothermal curves and the textural properties obtained from N_2 adsorption/desorption curves, impedance spectra of single cell with different cathode materials and different operating temperatures, XRD patterns, SEM images and N_2 adsorption/desorption curves for $La_{1.7}Ca_{0.3}Ni_{0.75}Cu_{0.25}O_{4-\delta}$ from conventional citric acid method. See DOI: 10.1039/c5ta00983a

high-temperature synthesis, as well as low stability with electrolytes.[34] Although some encouraging results have been reported, good evidence regarding SOFC cathode with high performance has not yet been available for this system.[33] For the purpose of this study, we have chosen these methods: doping Ca on the La-site and Ni substituting on the Cu-site, to enhance both the oxygen diffusion and their electrochemical performance as a cathode of IT-SOFCs.

Besides the composition, the microstructure of cathode also has influence on the electrochemical properties and performance of SOFCs.[35–38] Nanoscaled structure can accelerate oxygen reduction kinetics by providing enlarged number of active sites for surface oxygen exchange, which has great effect on the ORR of mixed ionic and electronic conductors.[36,37,39,40] Thus, in this study, we examined the applicability of the hierarchically nanostructured $La_{1.7}Ca_{0.3}Ni_xCu_{1-x}O_{4-\delta}$ $(0 \le x \le 0.75)$ cathode materials which were prepared by a facile citrate-modified evaporation-induced self-assembly (EISA) method or conventional citric acid method with the purpose of enhancing electrochemical performance under IT-SOFCs operating conditions, as well as investigating the effect of nanoparticle size on the performance. We systemically investigated the ratio of nickel to copper on the B-site of $La_{1.7}Ca_{0.3}Ni_xCu_{1-x}O_{4-\delta}$ $(0 \le x \le 0.75)$ and nanostructure morphologies with an effort to optimize their electrochemical properties. We report dramatically high power densities for the cell using nanostructured La_2CuO_4 series cathodes which are optimized their electrochemical properties with YSZ electrolyte.

Experimental section

Powder preparation

Hierarchically nanoporous $La_{1.7}Ca_{0.3}Ni_xCu_{1-x}O_{4-\delta}$ layered perovskite-type oxides were prepared by a citrate-modified EISA method. In a typical procedure, 2.0 g of Pluronic P123 (Mav = 5800, $EO_{20}PO_{70}EO_{20}$) was dissolved in 20 mL of ethanol and 5 mL of water at room temperature under vigorous magnetic stirring. Then 4.25 mmol of $La(NO_3)_3 \cdot 6H_2O$ (99.99%), 0.75 mmol of $Ca(NO_3)_2 \cdot 4H_2O$ (99.0%), and a total 2.5 mmol of B-site metal nitrates $Ni(NO_3)_2 \cdot 6H_2O$ (98+%) and $Cu(NO_3)_2 \cdot 2.5H_2O$ (≥98.0%)) were dissolved in the above solution under vigorous stirring, followed by adding 7.5 mmol of citric acid monohydrate (99.5%). The above mixture was covered with parafilm, stirred at room temperature for 5 h and then put in a drying oven (40 °C, relative humility below 40%) for solvent evaporation for about 4 days, followed by additional drying at 60 °C for 1 day and 80 °C for 12 h. Another type of nanostructured $La_{1.7}Ca_{0.3}Ni_{0.75}Cu_{0.25}O_{4-\delta}$ with a different particle size was prepared by a conventional citric acid method. In a typical process, 4.25 mmol of $La(NO_3)_3 \cdot 6H_2O$, 0.75 mmol of $Ca(NO_3)_2 \cdot 4H_2O$, 1.875 mmol of $(Ni(NO_3)_2 \cdot 6H_2O$ and 0.625 mmol of $Cu(NO_3)_2 \cdot 2.5H_2O$ were dissolved in a mixed solution of 20 mL ethanol and 10 mL H_2O under vigorous stirring, followed by adding 7.5 mmol of citric acid monohydrate. After stirred for 5 h, the solvent was evaporated at 90 °C under continuous stirring. The dried product was ground to a fine powder in a mortar and pestle and calcined in air at 300 °C for 3 h with the heating rate of 1 °C min^{-1}, followed by 750 °C for 2 h with 5 °C min^{-1}. The resulting products were used for coating cathode materials onto YSZ electrolyte. Part of the resulting product obtained from 750 °C was further calcined in air at 900 °C for 2 h to check their crystal structure and morphology change.

Fuel cell fabrication and testing

52 wt% NiO, 28 wt% YSZ powder (Praxair: SSA 56.4 m^2 g^{-1}) and 20 wt% graphite flake pore-former were mixed by roll mixing with the addition of 2-propanol solvent. Porous NiO–YSZ pallets were prepared by conventional pressing and firing at 1150 °C for 3 h. Then, a 55 wt% NiO–45 wt% YSZ slurry was dip-coated onto these sintered NiO–YSZ pallets to obtain a functional layer after firing at 1150 °C for 3 h. Followed, YSZ electrolyte was prepared by dip-coating YSZ ink onto the NiO–YSZ functional layer side of these sintered NiO–YSZ pallets. Finally, the pallets were heated at 1500 °C for 6 h to obtain NiO–YSZ supported YSZ electrolyte. $La_{1.7}Ca_{0.3}Ni_xCu_{1-x}O_{4-\delta}$ cathodes were prepared by hand painting nanostructured $La_{1.7}Ca_{0.3}Ni_xCu_{1-x}O_{4-\delta}$ powders onto electrolyte with 5 mm in diameter. The cathodes were then fired at 900 °C for 2 h in air. And, silver wire (0.25 mm, 99.99%, Advent Research Material Ltd) and silver paste (9912-G, ESL EUROPE) were employed for current collection.

For electrochemical performance and impedance measurements of the unit cell, Ni–YSZ|YSZ|$La_{1.7}Ca_{0.3}Ni_xCu_{1-x}O_{4-\delta}$, were performed in humidified H_2 and air or O_2 used as the fuels and oxidant, respectively, using an IM6 Electrochemical Workstation (ZAHNER, Germany) with frequency ranged from 0.1 Hz to 100 kHz with amplitude of 20 mV. Impedance plots were fitted using the Zview software.

Characterisation

Powder X-ray diffraction (XRD) patterns were recorded at room temperature on a PANalytical Empyrean Reflection Diffractometer using Cu Kα radiation (λ = 1.541 Å). The room-temperature crystal structure and the unit cell parameters were analyzed using the GSAS software. The morphologies of all samples and cells were observed on a JEOL JSM-6700 Field Scanning Electron Microscopy (FESEM). Transmission electron microscope (TEM) was performed using a JEOL JEM-2011 electron microscope at 200 kV. Nitrogen adsorption/desorption measurements were carried out under liquid nitrogen temperature (77 K) with a Tristar 3020 Instrument (Micrometrics Instrument Corp., Norcross, GA). The Brunauer–Emmett–Teller (BET) method was utilized to calculate the specific surface areas. By using the Barrett–Joyner–Halenda (BJH) model, the pore volumes and pore size distributions were derived from the adsorption branches of isotherms. The thermal expansion coefficient of the pellets in air was investigated using a Netzsch Model DIL 402 C instrument that was equipped with Proteus analysis software. Chemical compatibility between $La_{1.7}Ca_{0.3}Ni_xCu_{1-x}O_{4-\delta}$ cathode materials and YSZ electrolyte was evaluated by XRD analysis of an intimate mixture of 50 wt% $La_{1.7}Ca_{0.3}Ni_xCu_{1-x}O_{4-\delta}$ and 50 wt% YSZ fired at 900 °C for 5 h.

Results and discussion

Effect of $La_{1.7}Ca_{0.3}Ni_xCu_{1-x}O_{4-\delta}$ composition

The room-temperature phase structures of $La_{1.7}Ca_{0.3}Ni_xCu_{1-x}O_{4-\delta}$ ($x = 0$, 0.25, 0.50, 0.75) by the citrate-modified EISA method after calcination at 900 °C for 2 h under static air were studied by XRD analysis, as shown in Fig. 1. The XRD patterns show that all samples nearly display a pure phase pattern with tetragonal *I4/mmm* space group although traces of negligible secondary phases which can be indexed to $La_2CaCu_2O_6$ (JCPDS no. 43-0490) are observed in sample $La_{1.7}Ca_{0.3}CuO_{4-\delta}$ (Fig. 1a). The XRD patterns after final refinement using tetragonal *I4/mmm* model were shown in Fig. S1.† Their room-temperature lattice parameters *a* and *c*, and cell volume were summarized in Table 1. The *a* parameter increases slightly while the *c* parameter decreases significantly with the increasing Ni content in Cu-site, consistent with a decrease in the Jahn–Teller distortion for solid state samples induced by the presence of Cu(II) in the structure, similar to the reported results.[32] And the decrease in cell volume with the increasing Ni is considered resulting from the smaller ionic radii of Ni^{2+} ($r_{Ni^{2+}} = 0.69$ Å) than that of Cu^{2+} ($r_{Cu^{2+}} = 0.73$ Å). Their grain sizes were estimated from peaks (103), (110), (200) and (213) according to Scherrer equation and their average results were summarized in Table 1, indicating their nanostructures.

The chemical compatibility between $La_{1.7}Ca_{0.3}Ni_xCu_{1-x}O_{4-\delta}$ and YSZ after calcination at 900 °C for 5 h under static air was evaluated by XRD, as shown in Fig. 2. A lanthanum zirconate secondary phase ($La_2Zr_2O_7$, JCPDS no. 17-0450) can be observed in the cases of low nickel content ($x = 0$, 0.25 and 0.5) (Fig. 2a–c) and the intensity of this secondary phase increases with the Ni content increment. However, in the case of $La_{1.7}Ca_{0.3}Ni_{0.75}Cu_{0.25}O_{4-\delta}$, only traces of lanthanum zirconate can be detected, showing that substituting $La_{1.7}Ca_{0.3}CuO_{4-\delta}$ with 75% Ni on the B-site would prevent the formation of secondary phases. However, the detailed reasons for the different reactivity of these $La_{1.7}Ca_{0.3}Ni_xCu_{1-x}O_{4-\delta}$ materials with YSZ are still unclear, which need further investigation. Whilst no degradation would be preferred, the degree of degradation is probably acceptable for potential $La_{1.7}Ca_{0.3}Ni_xCu_{1-x}O_{4-\delta}$ electrodes at temperatures below 900 °C. Therefore, we have further analyzed the electrical and electrochemical properties as cathode materials of IT-SOFCs.

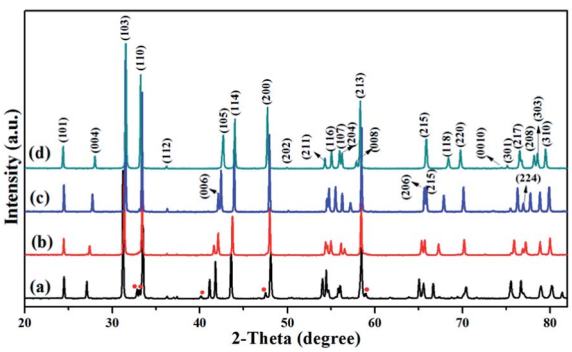

Fig. 1 XRD patterns of $La_{1.7}Ca_{0.3}Ni_xCu_{1-x}O_{4-\delta}$ calcined at 900 °C for 2 h in air: (a) $La_{1.7}Ca_{0.3}CuO_{4-\delta}$, (b) $La_{1.7}Ca_{0.3}Ni_{0.25}Cu_{0.75}O_{4-\delta}$, (c) $La_{1.7}Ca_{0.3}Ni_{0.5}Cu_{0.5}O_{4-\delta}$, (d) $La_{1.7}Ca_{0.3}Ni_{0.75}Cu_{0.25}O_{4-\delta}$. ● represents the impurity phase $La_2CaCu_2O_6$.

The SEM images of $La_{1.7}Ca_{0.3}Ni_xCu_{1-x}O_{4-\delta}$ samples calcined at 750 °C and 900 °C for 2 h in air are shown in Fig. 3 and S2.† Although the primary particle size is about 50–400 nm, these samples possess hierarchically nanoporous structures after calcination at 750 °C for 2 h, as shown in Fig. 3a–d.[41,42] This is maybe caused by the addition of P123 copolymer and citric acid during the synthesis process to favour the formation of hierarchically nanoporous layered perovskite oxides,[43,44] which would be expected to positively increase the electrochemical performance. Even on further sintering the samples (Fig. 3e–h) at 900 °C for 2 h, their hierarchically nanoporous structures are still maintained although the particle sizes are a bit bigger than those of samples obtained at 750 °C. Their TEM images displayed in Fig. S3† also show that these particles are inter-connected with each other to form hierarchically nanoporous structures, in agreement with their SEM results.

The textural properties of $La_{1.7}Ca_{0.3}Ni_xCu_{1-x}O_{4-\delta}$ samples after calcination at 750 °C and 900 °C for 2 h were evaluated by nitrogen adsorption/desorption. There are hysteresis loops between P/P_o of 0.9 and 1.0, as presented in Fig. S4,† corresponding to the secondary mesoporous/macroporous structures produced by inter-aggregated particles.[45,46] Their pore size distribution curves shown in Fig. S4† also demonstrate the co-existence of mesopores and macropores. Their BET specific surface areas (SSA), pore volume and average pore size calculated from N_2 adsorption isothermal curves were summarized in Table S1.† The results indicate that the BET SSA, pore volume and average pore size after calcination at 900 °C for 2 h are smaller than those of samples obtained at 750 °C for 2 h. However the BET SSA and pore volumes are still high for samples obtained at 900 °C. Consequently, these samples obtained at 750 °C and 900 °C could possess hierarchically mesoporous/macroporous nanostructures with high BET SSA and pore volumes, which are attributed to the large amount of secondary pores among particles, in agreement with the SEM and TEM results.

Table 1 Lattice parameters, cell volume and calculated grain sizes of $La_{1.7}Ca_{0.3}Ni_xCu_{1-x}O_{4-\delta}$ obtained from 900 °C for 2 h

Samples	*a* (Å)	*c* (Å)	Cell volume (Å^3)	Grain size (nm)
$La_{1.7}Ca_{0.3}CuO_{4-\delta}$	3.7875(3)	13.1897(5)	189.2124(5)	42.5
$La_{1.7}Ca_{0.3}Ni_{0.25}Cu_{0.75}O_{4-\delta}$	3.7916(6)	13.0185(8)	187.1647(2)	74.3
$La_{1.7}Ca_{0.3}Ni_{0.5}Cu_{0.5}O_{4-\delta}$	3.7958(9)	12.8831(2)	185.6306(9)	78.7
$La_{1.7}Ca_{0.3}Ni_{0.75}Cu_{0.25}O_{4-\delta}$	3.8109(3)	12.7415(7)	185.0488(5)	73.2

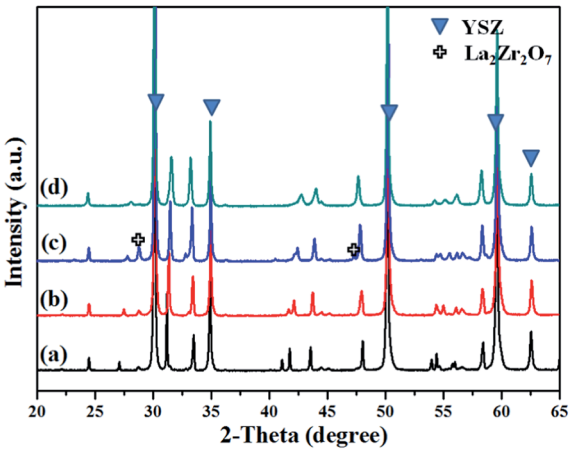

Fig. 2 XRD of $La_{1.7}Ca_{0.3}Ni_xCu_{1-x}O_{4-\delta}$–YSZ mixture calcined at 900 °C for 5 h: (a) $La_{1.7}Ca_{0.3}CuO_{4-\delta}$–YSZ, (b) $La_{1.7}Ca_{0.3}Ni_{0.25}Cu_{0.75}O_{4-\delta}$–YSZ, (c) $La_{1.7}Ca_{0.3}Ni_{0.5}Cu_{0.5}O_{4-\delta}$–YSZ, (d) $La_{1.7}Ca_{0.3}Ni_{0.75}Cu_{0.25}O_{4-\delta}$–YSZ.

In order to maintain the nanostructures, the hierarchically nanoporous cathode materials coated onto the YSZ electrolyte were fired at 900 °C for 2 h rather than being fired at higher temperature which would benefit the adherence between cathode and electrolyte if reaction could be avoided. The SEM images of the single cells using $La_{1.7}Ca_{0.3}Ni_xCu_{1-x}O_{4-\delta}$ oxides shown in Fig. S5† indicate that the hierarchically nanoporous structures of $La_{1.7}Ca_{0.3}Ni_xCu_{1-x}O_{4-\delta}$ cathode materials on the YSZ electrolyte were still remaining after sintering at 900 °C for 2 h. For all these four samples, the YSZ electrolyte is approximately 20 μm in thickness prepared by dip coating process and is adhered well to both cathode and anode layers without any delamination. The thickness of the $La_{1.7}Ca_{0.3}Ni_xCu_{1-x}O_{4-\delta}$ cathode materials is around 15–20 μm with a highly hierarchically nanoporous structure that favours the gas diffusion. These cathode materials all show small particle size even after heat-treatment at 900 °C for 2 h. Furthermore, these particles connected with one another, forming the secondary mesopores/macropores, which would increase the tri-phase boundaries to enhance the ORR on the cathode surfaces.

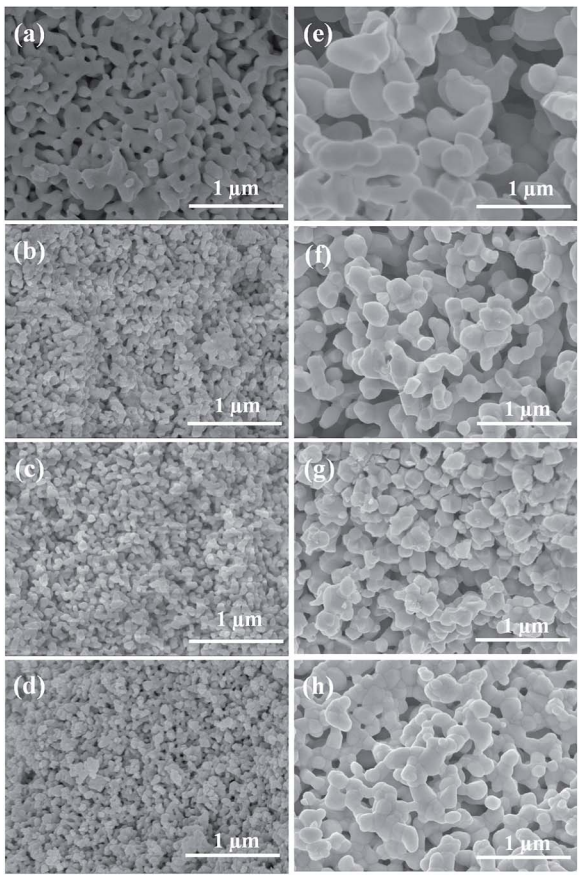

Fig. 3 SEM images of $La_{1.7}Ca_{0.3}Ni_xCu_{1-x}O_{4-\delta}$ after calcination at 750 °C (a–d) and 900 °C (e–h) for 2 h: (a and e) $La_{1.7}Ca_{0.3}CuO_{4-\delta}$, (b and f) $La_{1.7}Ca_{0.3}Ni_{0.25}Cu_{0.75}O_{4-\delta}$, (c and g) $La_{1.7}Ca_{0.3}Ni_{0.5}Cu_{0.5}O_{4-\delta}$, (d and h) $La_{1.7}Ca_{0.3}Ni_{0.75}Cu_{0.25}O_{4-\delta}$.

The power generation property of the cells using the $La_{1.7}Ca_{0.3}Ni_xCu_{1-x}O_{4-\delta}$ powder as cathode, humidified H_2 as fuel and air as oxidant, respectively, with respect to the temperature, for the Ni–YSZ support and YSZ electrolyte systems is shown in Fig. 4. The maximum power densities (MPD) of the cells with the $La_{1.7}Ca_{0.3}Ni_xCu_{1-x}O_{4-\delta}$ ($x = 0$, 0.25, 0.50, and 0.75) cathode materials were summarized in Fig. 5, in which their MPD at 850 °C were 1.5, 0.67, 0.74 and 0.89 W cm^{-2}, respectively. Compared to previous data on electrochemical performance of cuprate cathodes fabricated at higher temperature,[32] much improved performance is achieved by the hierarchically nanoporous $La_{1.7}Ca_{0.3}CuO_{4-\delta}$ cathode. This suggests that low-temperature ceramic processing to fabricate nanostructured cathode layer offer a suitable potential on the cuprate cathode of SOFCs to effectively overcome its lower chemical compatibility in the long term. For $La_{1.7}Ca_{0.3}Ni_xCu_{1-x}O_{4-\delta}$ ($x = 0.25$, 0.50, and 0.75) samples, their power density slightly increased with Ni content over the whole temperature range, which can be attributed to their increased oxygen ion mobility with Ni content. The highest MPD achieved by the $La_{1.7}Ca_{0.3}CuO_{4-\delta}$ cathode at high temperature range can be attributed to its high electrical conductivity while doping La-site with Ca would result in enhanced oxygen ion mobility by the formation of oxygen vacancies and/or interstitial oxygen.[28,31] As shown in Fig. 5, the MPD of $La_{1.7}Ca_{0.3}Ni_{0.75}Cu_{0.25}O_{4-\delta}$ was slightly higher than that of $La_{1.7}Ca_{0.3}CuO_{4-\delta}$ at lower temperatures (*e.g.*, 700 and 750 °C). The MPD of $La_{1.7}Ca_{0.3}Ni_{0.75}Cu_{0.25}O_{4-\delta}$ cathode achieved 0.51 and 0.71 W cm^{-2} at 700 and 750 °C, respectively.

In order to further study the cathodic polarization (R_p) during cell performance, impedance spectroscopy results were considered, taking the impedance intercept of high, mid and low frequency with the real axis of the Nyquist plot in order to determine the ohmic resistance (R_s) and non-ohmic resistance (R_p total $= R_{p1} + R_{p2} + R_{p3}$). Fig. 6 shows the impedance spectra of the cell, Ni–YSZ|YSZ|$La_{1.7}Ca_{0.3}CuO_{4-\delta}$, with simulated fitting curve under open circuit conditions at 700 °C and the whole impedance spectra for $La_{1.7}Ca_{0.3}Ni_xCu_{1-x}O_{4-\delta}$ as thermal variation were represented in Fig. S6 and S7.† As shown in Fig. 6, two or three semicircles were roughly observed on impedance fitting plot and considering response frequency, semicircle at

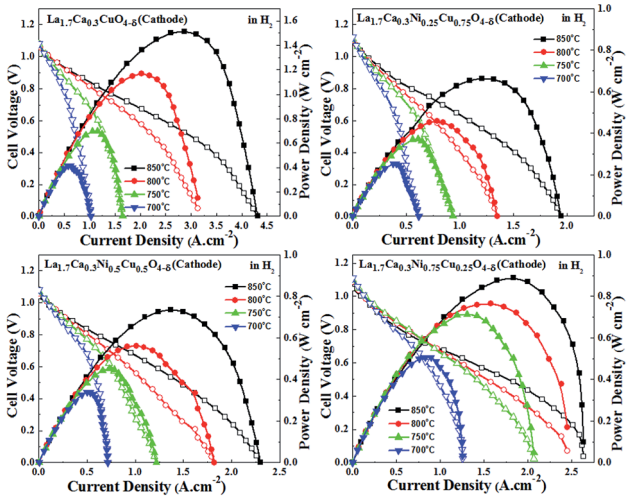

Fig. 4 Single cell performance of a cell with $La_{1.7}Ca_{0.3}Ni_xCu_{1-x}O_{4-\delta}$ (x = 0, 0.25, 0.50, and 0.75) cathodes at various temperatures using humidified H_2 and air as the fuel and oxidant, respectively.

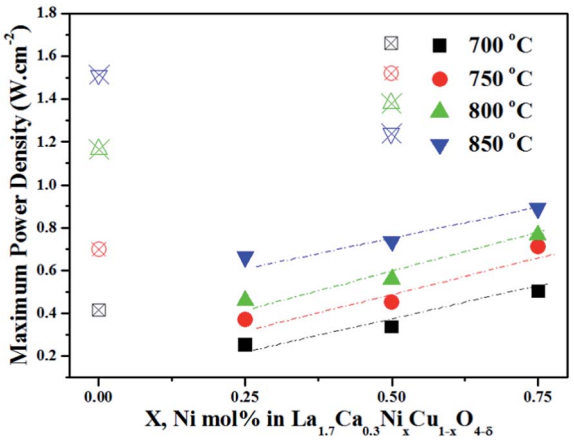

Fig. 5 Maximum power density as a function of Ni content of $La_{1.7}Ca_{0.3}Ni_xCu_{1-x}O_{4-\delta}$ (x = 0, 0.25, 0.50, and 0.75) cathodes using humidified H_2 and air as the fuel and oxidant, respectively.

high (R_{p1}) and mid frequency (R_{p2}) could be assigned to the surface activation, oxygen and charge transfer while lower frequency (R_{p3}) should be associated with gas diffusion. Clearly the high frequency interception (R_s) is barely changed or slightly decreased by elevating temperature because ohmic resistance mainly arises from electrolyte.

Fig. 7a and b show Arrhenius plots of the thermal variation area-specific resistance (ASR) for ohmic and non-ohmic, respectively. As shown in Fig. 7c, activation energy for R_{p1} and R_{p2} were dramatically decreased with the increase of Ni content on the Cu-site which can be due to the increased oxygen overstoichiometry, similar to that of $La_2Ni_{1-x}Cu_xO_{4+\delta}$.[47] The slight improvement of electrochemical performance (*e.g.*, MPD) with Ni–Cu couple might also reflect the changing of anisotropic oxygen transport mechanism (*e.g.*, orthorhombic distortion, Jahn–Teller distortion of Cu^{2+}, increased oxygen vacancies) in

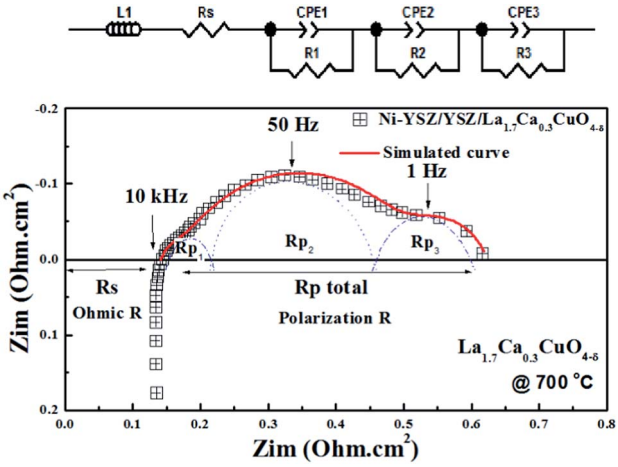

Fig. 6 Impedance spectra measured for a cell using Ni–YSZ|YSZ|$La_{1.7}Ca_{0.3}CuO_{4-\delta}$ at 700 °C and simulated fitting by Zview software.

tetragonal layered perovskite structure with respect to Ni contents.[47] For $La_{1.7}Ca_{0.3}CuO_{4-\delta}$, it also exhibits structural distortion and oxygen content change with the increasing of temperature, which may contribute to its excellent performance at high temperatures.[28] On the other hand, the slight increase of activation energy for R_{p3} with increasing Ni is because R_{p3} would be related with microstructure factor and gas diffusion in electrode. Accordingly, nanoporous factor, as shown in Table S1,† might be in reasonable agreement with R_{p3} polarization result. Considering the same anode and electrolyte for these cells, excepting $La_{1.7}Ca_{0.3}CuO_{4-\delta}$, it can be concluded that Ni–Cu couple of octahedral site in layered perovskite improves surface reactivity for oxygen transfer. In addition, the thermal expansion coefficient (TEC) values of $La_{1.7}Ca_{0.3}Ni_xCu_{1-x}O_{4-\delta}$ were reduced with the increasing Ni contents in Cu site, suggesting $La_{1.7}Ca_{0.3}Ni_{0.75}Cu_{0.25}O_{4-\delta}$ cathode shows relatively adaptable thermal compatibility with the typical SOFC electrolyte materials, as shown in Table 2. Therefore, considering a better stability, lower operating temperature, higher MPD at low temperature and more suitable TEC, hierarchically nanoporous $La_{1.7}Ca_{0.3}Ni_{0.75}Cu_{0.25}O_{4-\delta}$ would be promising as a potential cathode for IT-SOFCs.

Effect of cathode particle size and morphology

As discussed in aforementioned paragraphs, $La_{1.7}Ca_{0.3}Ni_{0.75}Cu_{0.25}O_{4-\delta}$ shows the highest powder density during intermediate-temperature range (≤750 °C). To further investigate the effect of particle size and morphology on the electrochemical performance, we prepared another kind of $La_{1.7}Ca_{0.3}Ni_{0.75}Cu_{0.25}O_{4-\delta}$ using conventional citric acid method for comparison. The XRD patterns and SEM images in Fig. S8† for $La_{1.7}Ca_{0.3}Ni_{0.75}Cu_{0.25}O_{4-\delta}$ using conventional citric acid method after calcination at 750 or 900 °C for 2 h demonstrated their pure tetrahedral structure with *I*4/*mmm* space group and hierarchical nanostructures. The calculated average grain size from the XRD pattern of $La_{1.7}Ca_{0.3}Ni_{0.75}Cu_{0.25}O_{4-\delta}$ synthesized by conventional citric acid method at 900 °C in Fig. S8a† is

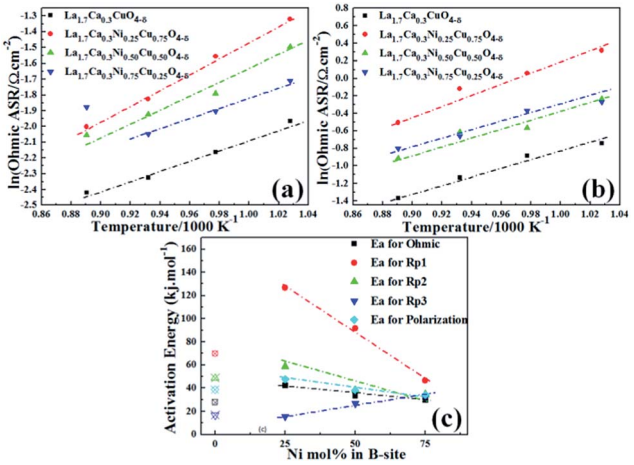

Fig. 7 ASR temperature dependence and activation energies for various cathodes, $La_{1.7}Ca_{0.3}Ni_xCu_{1-x}O_{4-\delta}$: (a) Arrhenius plot for ohmic resistance, R_s; (b) for non-ohmic resistance, R_p total = $R_{p1} + R_{p2} + R_{p3}$; and (c) activation energies of them.

Table 2 Thermal expansion coefficient (TEC, 10^{-6} K^{-1}) values for the $La_{1.7}Ca_{0.3}Ni_xCu_{1-x}O_{4-\delta}$ ($x = 0$, 0.25, 0.5, 0.75)

Samples	TEC_{50-850}
$La_{1.7}Ca_{0.3}CuO_{4-\delta}$	15.4
$La_{1.7}Ca_{0.3}Ni_{0.25}Cu_{0.75}O_{4-\delta}$	15.2
$La_{1.7}Ca_{0.3}Ni_{0.5}Cu_{0.5}O_{4-\delta}$	14.9
$La_{1.7}Ca_{0.3}Ni_{0.75}Cu_{0.25}O_{4-\delta}$	14.4
8YSZ (ZrO_2 with 8 mol% Y_2O_3)	10.7
LSGM ($La_{0.9}Sr_{0.1}Gd_{0.8}Mg_{0.2}O_{3-\delta}$)	11.8
CGD ($Ce_{0.9}Gd_{0.1}O_{2-\delta}$)	13.2

about 60.3 nm, which is smaller than that (*i.e.*, 73.2 nm) of $La_{1.7}Ca_{0.3}Ni_{0.75}Cu_{0.25}O_{4-\delta}$ by citrate-modified EISA method. The SEM images in Fig. S8b and c† indicate the growth of particle size with the increasing of calcination temperature, but still maintaining nanostructured morphology after calcination at 900 °C for 2 h. The N_2 adsorption/desorption curves shown in Fig. S9† demonstrated the smaller BET surface areas and pore volumes in the $La_{1.7}Ca_{0.3}Ni_{0.75}Cu_{0.25}O_{4-\delta}$ prepared by conventional citric acid method than that by citrate-modified EISA method.

The single cells were prepared by using Ni–YSZ|YSZ anode supported electrolyte, in which the thickness of electrolyte is *ca.* 30 μm. The cells were tested using pure H_2 and O_2 as the fuel and oxidant, respectively. The electrochemical performance, OCV, and MPD of the cells with $La_{1.7}Ca_{0.3}Ni_{0.75}Cu_{0.25}O_{4-\delta}$ cathodes are shown in Fig. 8. The results indicate that $La_{1.7}Ca_{0.3}Ni_{0.75}Cu_{0.25}O_{4-\delta}$ cathode prepared by citrate-modified EISA method shows a bit higher MPD than that of $La_{1.7}Ca_{0.3}Ni_{0.75}Cu_{0.25}O_{4-\delta}$ by conventional citric acid method during the whole temperature range, especially at low temperature (*e.g.*, 750 °C), suggesting its higher ORR activity at low temperature based on the consideration of the same Ni–YSZ anode and YSZ electrolyte for these two cells. However, with the increasing of testing temperature, the difference between the two cathodes decreased and their MPD are almost the same at 850 °C, indicating high ORR activity in both cathode samples at 850 °C. However, during the whole testing temperature range, the OCV values are relatively higher when using $La_{1.7}Ca_{0.3}Ni_{0.75}Cu_{0.25}O_{4-\delta}$ obtained by citrate-modified EISA method as cathode, as shown in Fig. 8c, which might be obviously caused by its bigger grain size, higher surface area, pore volume and surface activity for ORR.

The impedance spectra, IR loss and overpotential η are displayed in Fig. 9. The results in Fig. 9a and b show that the R_p is a bit smaller when using $La_{1.7}Ca_{0.3}Ni_{0.75}Cu_{0.25}O_{4-\delta}$ from citrate-modified EISA method as cathode materials while there were no obvious differences in non-ohmic resistance. The smaller R_p can be attributed to the improved oxygen ion mobility due to its bigger grain size. However, the overpotential η results shown in Fig. 9c indicate that the total overpotential η in the single cell using $La_{1.7}Ca_{0.3}Ni_{0.75}Cu_{0.25}O_{4-\delta}$ from citrate-modified EISA method as cathode was smaller than that from conventional citric acid method. It might be attributed to the more three-phase boundary active site, and better oxygen ion mobility and adhesion between electrolyte and the $La_{1.7}Ca_{0.3}Ni_{0.75}Cu_{0.25}O_{4-\delta}$ cathode from citrate-modified EISA method, since it has a bit bigger grain size, higher surface area and pore volume. However, which is the predominating effect, grain size, surface area or pore volume, is still under investigation.

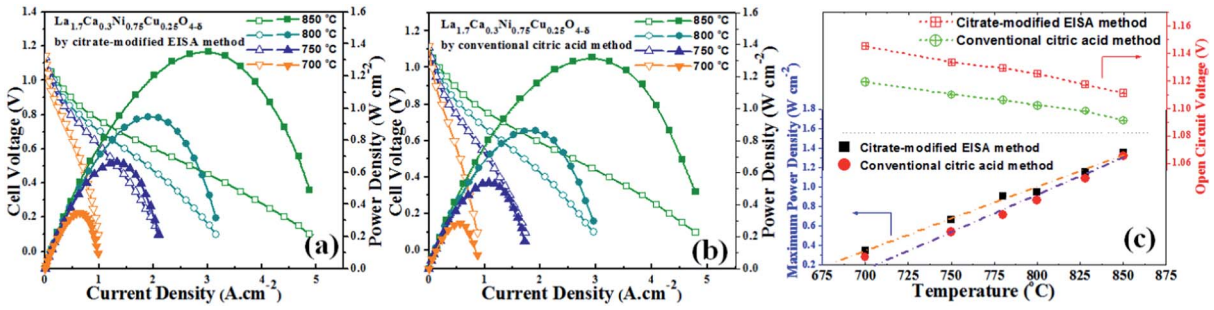

Fig. 8 Single cell performance (a and b), OCV and MPD (c) of a cell with $La_{1.7}Ca_{0.3}Ni_{0.75}Cu_{0.25}O_{4-\delta}$ cathodes at various temperatures using pure H_2 and O_2 as the fuel and oxidant, respectively.

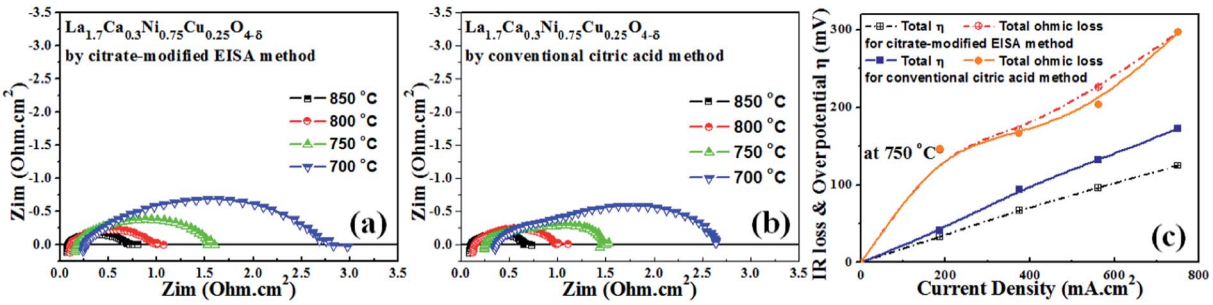

Fig. 9 Impedance spectra (a and b), and IR loss and & overpotential η of $La_{1.7}Ca_{0.3}Ni_{0.75}Cu_{0.25}O_{4-\delta}$ cathodes.

Conclusions

In summary, hierarchically nanoporous layered perovskite oxides $La_{1.7}Ca_{0.3}Ni_xCu_{1-x}O_{4-\delta}$ ($0 \leq x \leq 0.75$) with pure phases have been successfully synthesized by a facile citrate-modified EISA method at low temperature, in which copolymer P123 and citric acid are used together to produce hierarchical nanopores. They can maintain their nanostructures with high surface areas even after calcination at 900 °C for 2 h. The electrochemical results from Ni–YSZ supported IT-SOFCs using humidified H_2 as fuel and air as oxidant show that $La_{1.7}Ca_{0.3}Ni_xCu_{1-x}O_{4-\delta}$ ($0 \leq x \leq 0.75$) display acceptable electrochemical performance, in which $La_{1.7}Ca_{0.3}CuO_{4-\delta}$ as cathode material displays the best performance (*e.g.*, 1.2 and 1.5 W cm^{-2} at 800 and 850 °C, respectively). However, its performance at intermediate temperatures is lower than that of $La_{1.7}Ca_{0.3}Ni_{0.75}Cu_{0.25}O_{4-\delta}$ cathode material (*e.g.*, 0.71 W cm^{-2} at 750 °C). In addition, $La_{1.7}Ca_{0.3}Ni_{0.75}Cu_{0.25}O_{4-\delta}$ cathode material with smaller grain size and surface areas from conventional citric acid method exhibited worse electrochemical performance than that prepared by citrate-modified EISA method at the whole temperature range (700–850 °C), especially low temperature (*e.g.*, 750 °C), demonstrating the positive effect of hierarchically nanoporous structure with higher surface areas and bigger grain size of cathode materials on the electrochemical performance. Therefore, hierarchically nanoporous $La_{1.7}Ca_{0.3}Ni_{0.75}Cu_{0.25}O_{4-\delta}$ would be promising as a potential cathode for IT-SOFCs due to its better stability, higher MPD at low temperature and more suitable TEC with electrolyte.

Acknowledgements

The authors gratefully thank the Engineering and Physical Sciences Research Council (EPSRC) platform grant EP/I022570/1 and EP/I022570/2 for financial support.

Notes and references

1 A. B. Stambouli and E. Traversa, *Renewable Sustainable Energy Rev.*, 2002, **6**, 433–455.
2 N. Q. Minh, *Solid State Ionics*, 2004, **174**, 271–277.
3 B. C. H. Steele and A. Heinzel, *Nature*, 2001, **414**, 345–352.
4 Z. Shao and S. M. Haile, *Nature*, 2004, **431**, 170–173.
5 J. H. Kim, M. Cassidy, J. T. S. Irvine and J. Bae, *Chem. Mater.*, 2010, **22**, 883–892.
6 J. Chen, F. Liang, L. Liu, S. P. Jiang and L. Jian, *Int. J. Hydrogen Energy*, 2009, **34**, 6845–6851.
7 D. J. L. Brett, A. Atkinson, N. P. Brandon and S. J. Skinner, *Chem. Soc. Rev.*, 2008, **37**, 1568–1578.
8 C.-D. Savaniu and J. T. S. Irvine, *J. Mater. Chem.*, 2009, **19**, 8119–8128.
9 H. S. Isaacs and L. J. Olmer, *J. Electrochem. Soc.*, 1982, **129**, 436–443.
10 Y. Takeda, R. Kanno, M. Noda, Y. Tomida and O. Yamamoto, *J. Electrochem. Soc.*, 1987, **134**, 2656–2661.
11 S. Yoo, J. Y. Shin and G. Kim, *J. Mater. Chem.*, 2011, **21**, 439–443.
12 L. Zhao, B. He, Y. ling, Z. Xun, R. Peng, G. Meng and X. Liu, *Int. J. Hydrogen Energy*, 2010, **35**, 3769–3774.
13 W. Lee, J. W. Han, Y. Chen, Z. Cai and B. Yildiz, *J. Am. Chem. Soc.*, 2013, **135**, 7909–7925.
14 H. Jalili, J. W. Han, Y. Kuru, Z. Cai and B. Yildiz, *J. Phys. Chem. Lett.*, 2011, **2**, 801–807.
15 S. Jiang, *J. Solid State Electrochem.*, 2007, **11**, 93–102.
16 H. P. Ding, A. V. Virkar, M. L. Liu and F. Liu, *Phys. Chem. Chem. Phys.*, 2013, **15**, 489–496.
17 W. Jung and H. L. Tuller, *Energy Environ. Sci.*, 2012, **5**, 5370–5378.
18 Y. Chen, W. Jung, Z. H. Cai, J. J. Kim, H. L. Tuller and B. Yildiz, *Energy Environ. Sci.*, 2012, **5**, 7979–7988.
19 I. Riess, *Solid State Ionics*, 2003, **157**, 1–17.
20 A. Tarancon, M. Burriel, J. Santiso, S. J. Skinner and J. A. Kilner, *J. Mater. Chem.*, 2010, **20**, 3799–3813.
21 A. Aguadero, L. Fawcett, S. Taub, R. Woolley, K.-T. Wu, N. Xu, J. Kilner and S. Skinner, *J. Mater. Sci.*, 2012, **47**, 3925–3948.
22 V. V. Kharton, A. P. Viskup, E. N. Naumovich and F. M. B. Marques, *J. Mater. Chem.*, 1999, **9**, 2623–2629.
23 Y. Takeda, R. Kanno, M. Sakano, O. Yamamoto, M. Takano, Y. Bando, H. Akinaga, K. Takita and J. B. Goodenough, *Mater. Res. Bull.*, 1990, **25**, 293–306.
24 Y. Shen, H. Zhao, X. Liu and N. Xu, *Phys. Chem. Chem. Phys.*, 2010, **12**, 15124–15131.
25 J. Zhou, G. Chen, K. Wu and Y. Cheng, *J. Phys. Chem. C*, 2013, **117**, 12991–12999.
26 A. Aguadero, J. A. Alonso, M. J. Martinez-Lope, M. T. Fernandez-Diaz, M. J. Escudero and L. Daza, *J. Mater. Chem.*, 2006, **16**, 3402–3408.

27 J. P. Attfield, A. L. Kharlanov and J. A. McAllister, *Nature*, 1998, **394**, 157–159.
28 L. Shen, P. Salvador, T. O. Mason and K. Fueki, *J. Phys. Chem. Solids*, 1996, **57**, 1977–1987.
29 Q. Li, H. Zhao, L. Huo, L. Sun, X. Cheng and J.-C. Grenier, *Electrochem. Commun.*, 2007, **9**, 1508–1512.
30 G. N. Mazo and S. N. Savvin, *Solid State Ionics*, 2004, **175**, 371–374.
31 C. Rial, E. Morán, M. A. Alario-Franco, U. Amador, J. L. Martínez, J. Rodríguez-Carvajal and N. H. Andersen, *Phys. C*, 1998, **297**, 277–293.
32 A. Aguadero, J. A. Alonso, M. J. Escudero and L. Daza, *Solid State Ionics*, 2008, **179**, 393–400.
33 Y. Shen, H. Zhao, K. Świerczek, Z. Du and Z. Xie, *J. Power Sources*, 2013, **240**, 759–765.
34 R. Ruiz-Bustos, A. Cantos-Gómez, A. J. Dos santos-García, C. Sánchez-Bautista and J. van Duijn, *Fuel Cells*, 2011, **11**, 59–64.
35 Z. Jiang, C. Xia and F. Chen, *Electrochim. Acta*, 2010, **55**, 3595–3605.
36 S. P. Jiang, *Mater. Sci. Eng., A*, 2006, **418**, 199–210.
37 C. Ding and T. Hashida, *Energy Environ. Sci.*, 2010, **3**, 1729–1731.
38 H. S. Song, S. H. Hyun, J. Kim, H.-W. Lee and J. Moon, *J. Mater. Chem.*, 2008, **18**, 1087–1092.
39 E. D. Wachsman and K. T. Lee, *Science*, 2011, **334**, 935–939.
40 M. Zhi, S. Lee, N. Miller, N. H. Menzler and N. Wu, *Energy Environ. Sci.*, 2012, **5**, 7066–7071.
41 Z.-Y. Yuan and B.-L. Su, *J. Mater. Chem.*, 2006, **16**, 663–677.
42 J.-L. Blin, A. Léonard, Z.-Y. Yuan, L. Gigot, A. Vantomme, A. K. Cheetham and B.-L. Su, *Angew. Chem.*, 2003, **115**, 2978–2981.
43 H. Chen, J. Gu, J. Shi, Z. Liu, J. Gao, M. Ruan and D. Yan, *Adv. Mater.*, 2005, **17**, 2010–2014.
44 Y. Huang, H. Cai, D. Feng, D. Gu, Y. Deng, B. Tu, H. Wang, P. A. Webley and D. Zhao, *Chem. Commun.*, 2008, 2641–2643.
45 W. Ho, J. C. Yu and S. Lee, *Chem. Commun.*, 2006, 1115–1117.
46 L. Zhang and J. C. Yu, *Chem. Commun.*, 2003, 2078–2079.
47 E. Boehm, J. M. Bassat, M. C. Steil, P. Dordor, F. Mauvy and J. C. Grenier, *Solid State Sci.*, 2003, **5**, 973–981.